Energy 254 (2022) 124319

Contents lists available at ScienceDirect

Energy

journal homepage: www.elsevier.com/locate/energy

A computational drop-in assessment of hydrofluoroethers in Organic Rankine Cycles

Daniel Jovell [a], Rafael Gonzalez-Olmos [a], Fèlix Llovell [b, *]

[a] Department of Chemical Engineering and Materials Science, IQS School of Engineering, Universitat Ramon Llull, Via Augusta 390, 08017, Barcelona, Spain
[b] Department of Chemical Engineering, ETSEQ, Universitat Rovira i Virgili, Avinguda Països Catalans 26, 43007, Tarragona, Spain

ARTICLE INFO

Article history:
Received 28 February 2022
Received in revised form
10 May 2022
Accepted 16 May 2022
Available online 19 May 2022

Keywords:
Hydrofluoroethers
Organic Rankine Cycle
Drop-in replacement
Polar soft-SAFT
Thermal efficiency
Energy consumption

ABSTRACT

Organic Rankine Cycles (ORCs) are experiencing a growing interest due to their ability to generate electricity from residual low waste heat sources. HFC-245fa is a representative working fluid for ORC applications, but it has recently been phased-out in new equipment because of its high global warming potential (GWP). In this work, the soft-SAFT molecular-based equation of state is used to evaluate the capacity of nine promising low-GWP hydrofluoroethers (HFEs) as alternative working fluids in ORC applications using different key performance indicators focused on energy efficiency and service fluids consumption. The thermodynamic model has been employed to characterize these fluids by describing saturated densities, vapor pressure, surface tension, temperature-enthalpy, and temperature-entropy diagrams, including further validation with binary mixtures. Then, based on technical criteria focused on the thermal efficiency and working and service fluids consumption, the soft-SAFT model has been used to conduct a feasibility study of HFEs as direct substitutes for HFC-245fa in such applications. Although pure fluids can not reach the same efficiency as the benchmark, HFE-356mmz, HFE-7000, and HFE-7100 appear as promising replacements, capable of approaching system requirements operating at low pressure with low cooling water and heating fluid flow rates, while exhibiting lower GWP values.

1. Introduction

The United Nations Climate Change Conference (COP 26) held in Glasgow in 2021, underlined the urgency and potential of transitioning towards a carbon-free economy and urged transparency and rigor in climate action plans from both governments and companies. Still, the world remains off-track to beat back the climate crisis; ministers from nations such as the United States and India agreed that additional reductions in hydrofluorocarbons (HFCs) emissions, as well as other climate pollutants like methane and black carbon, are required to keep global warming below 1.5 °C and avoid millions of early deaths due to air pollution. According to the Climate and Clean Air Coalition (CCAC) approach, HFCs must be *nearly eradicated* by 2050, with a reduction of 99.5% respect to the 2010 levels [1].

Organic Rankine Cycles (ORCs) are presented as an effective way to minimize fossil fuel usage and greenhouse gas emissions, as they can recover the heat discharged in power plants from flue gas, drained water, and exhaust steam to generate electricity. In ORCs, organic fluids, including fluorinated refrigerants, are typically used as working fluids for low-temperature waste-heat recovery [2]. HFCs stand out as the dominant working fluids among the different refrigerants, being HFC-245fa (1,1,1,3,3-Pentafluoropropane) the most suitable one used in the industry [3–6]. However, the strict European regulations, such as EU no. 517/2014, or the Kigali amendment to the Montreal Protocol [7,8], are in the path of the CCAC conclusions and are phasing out the use of high global warming potential (GWP) refrigerants, such as HFC-245fa (GWP = 962 kg CO_2 eq [9]), whose commercialization has been banned as of January 1st, 2022, in Europe [8].

The challenge in finding a replacement for the working fluids now in use stems not only from the need to identify an alternative compound with similar thermophysical properties, but also to evaluate the environmental effects, flammability, toxicity, and material compatibility of the new fluid. Among the possible replacements of HFC-245fa, two different families of compounds have been identified. Firstly, hydrofluoroolefins (HFOs) and

* Corresponding author.
E-mail address: felix.llovell@urv.cat (F. Llovell).

https://doi.org/10.1016/j.energy.2022.124319

hydrochlorofluoroolefins (HCFOs) have been investigated in the literature as potential replacements for HFC-245fa in current ORC systems [10–13]. Among these, HCFO-1233zd(E) (*trans*-1-Chloro-3,3,3-trifluoropropene), a non-flammable ultra-low GWP (3.88 kg CO_2 eq.) compound, has been stated as a suitable drop-in replacement for HFC-245fa [2–5,14,15]. Eyerer and coworkers conducted an experimental study in an ORC test rig and concluded that HCFO-1233zd(E) can effectively replace HFC-245fa and may even result in higher thermal efficiencies, although particular care on the lubricant choice and the material compatibility of all the components in contact with the refrigerant (especially in sealing materials), should be considered [14]. Other working fluids studied include HFO-1234ze(Z) ((1*Z*)-1,3,3,3-Tetrafluoro-1-propene) [6], HFO-1336mzz(E) (*trans*-1,1,1,4,4,4-Hexafluoro-2-butene) [5], and HCFO-1224yd ((1*Z*)-1-Chloro-2,3,3,3-tetrafluoro-1-propene) [4]. While the first compound has been proved to be a suitable drop-in replacement for HFC-245fa in ORC applications, further studies are required to evaluate whether the others may fulfill the requirements for such applications. The reader is referred to the individual contributions for further details [4–6].

Secondly, hydrofluoroethers (HFEs) have also been stated as alternative working fluids to HFCs for ORCs [16–20]. HFEs exhibit similar physicochemical properties compared to HFCs, including high volatility, low thermal conductivity, surface tension, toxicity and flammability, and zero ozone depletion potential (ODP) [19]. Moreover, the addition of the ether group in its chemical structure lowers the atmospheric lifespan, decreasing their GWPs. Indeed, the thermodynamic, environmental and safety analysis based on the spinal point method carried out by Qiu [17] for 8 different working fluids recommends HFE-7000 and HFE-7100 as preferred over other HFC, hydroclorofluorocarbon (HCFC) and perfluorocarbon (PFC) alternatives. In this regard, both the US Environmental Protection and the European Environmental Agencies have suggested replacing HFCs with HFEs [21].

To our knowledge, only two contributions have addressed the feasibility of HFEs as alternative working fluids in ORCs in the literature [18,20]. In particular, it is worthy to highlight the work of Jang and Lee [20]. In this contribution, the authors built four different micro combined heat and power (CHP) thermodynamic models and determined the best-operating conditions for three different working fluid groups, including two HFEs (HFE-7000 and HFE-7100). The results suggested that these two HFEs might be used as alternative working fluids, albeit the ORC configuration strongly impacts the fluid's choice.

An accurate analysis of the use of HFEs as efficient substitutes for HFC-245fa requires a detailed thermophysical characterization to fully understand the behavior of these fluids in the ORC's operating conditions. While some properties, such as liquid density and vapor pressure, have been reported for most fluids, this information is limited to specific temperature and pressure ranges. In addition, there is a lack of standardized information of other key data, such as enthalpies and entropies. The absence of a comprehensive experimental characterization can be addressed using computational strategies with the capacity to quickly identify suitable HFCs' substitutes, while meeting environmental and technological constraints in an efficient, cost-saving and reliable way. In this context, molecular-based equations of state (EoS), such as those derived from the Statistical Association Fluid Theory (SAFT) [22] have become crucial tools for simulating complex fluid thermodynamic behavior and energy calculations. The soft-SAFT EoS [23] has been widely used to describe the thermodynamic behavior of complex fluids for applications in climate change mitigation, including the modeling of solvents for CO_2 capture [24,25] or the thermophysical characterization of 3rd generation HFCs refrigerants [26–28] for their recovery and subsequent substitution by unsaturated low-GWP fluorinated compounds like HFOs and HCFOs [29,30]. The models built under the soft-SAFT framework have a solid base on statistical mechanics and are capable of correctly capturing the influence of intermolecular interactions using coarse-grained models, which can be then used for process modeling. This is an advantage over other conventional EoS, which are unable to capture the polar interactions that predominate in this type of compounds. However, the application to model HFEs is scarce, with only a few contributions covering 3 M™'s Novec Engineered Fluids (e.g., HFE-7000, HFE-7100, HFE-7200, HFE-7300, and HFE-7500). In particular, Vijande et al. [31] described the PVT behavior of several HFEs based on available experimental data and proposed a group contribution scheme from the perturbed-chain PC-SAFT EoS variant to extrapolate the parameters for other molecules of the same family. Similarly, Vinš et al. [21] developed a PCP-SAFT model, including polar effects, for the aforementioned HFEs, where the density gradient theory was coupled to estimate the surface tension. Other approaches combining the SAFT-VR version with a group contribution approach are also under study [32].

The use of molecular modeling tools allow a complete description of the thermophysical properties of HFEs, which may provide handy information regarding their intermolecular interactions. This would expand the analysis of alternative working fluids in ORCs for potential drop-in candidates, which is the case of the outstanding contributions of Markides' research group, who have successfully employed the SAFT-γ-Mie EoS to address the performance of several working fluids, including fluorocarbons [33] and hydrocarbons [34,35], both from a process and economic point of view.

However, to our knowledge, no work addresses the use of SAFT models for the screening of alternative HFE working fluids to low-grade waste heat recovery ORCs, extending the thermodynamic characterization to fluids other than 3M's, that are theorized to be possible replacements. More importantly, this information has not been used to accurately assess the actual efficiency of these fluids in terms of energy yield.

In this work, a low-grade waste heat recovery ORC has been simulated and its conditions optimized for a selection of nine different potential HFE working fluids as alternatives to HFC-245fa (benchmark), all of them listed in Table 1. The choice is based on the condition of a lower GWP than the benchmark fluid. The soft-SAFT EoS [36] has been used for the first time to model these compounds, specifically including the impact of the permanent dipole of these molecules for a more realistic and reliable prediction of their thermophysical behavior. Based on such optimization, the performance of each compound has been evaluated in terms of thermal efficiency and cooling water, heating fluid, and working fluid consumption, providing new insight into the feasibility of using HFEs as drop-in replacements for ORCs.

2. ORC process simulation

The scheme of the modeled single ORC is shown in Fig. 1, with the corresponding T-S diagram. This basic configuration comprises a feed pump, an evaporator, an expander, and a condenser. The saturated liquid is pressurized in the pump and evaporated in the evaporator exchanger in the considered implementation. The saturated vapor is pushed through an expander and a condenser, where it is cooled and liquefied, restarting the cycle.

A 2 K subcooling temperature was set in the condenser to ensure complete liquid phase at the input of the pump to avoid damage. However, superheating was not considered at the evaporator's outlet because droplets in metastable pure vapor state are not expected under saturated conditions [44–46]. Following Jang and Lee's study [20], heat and head losses were assumed to be

Table 1
Selection of working fluids studied in this work and their main characteristics.

NAME	Other identifiers	CAS	Molecular weight	Boiling point (K)[a]	Critical temperature (K)[a]	Critical Pressure (MPa)[a]	Enthalpy of vaporization at 293.15 K[b] (kJ/kg)	Flammability limits[c]	GWP[d]
1,1,1,3,3-Pentafluoropropane	HFC-245fa	460-73-1	134.05	288.25	427.10	3.654	192.52	Non-flammable	962.0
Trifluoromethyl Methyl Ether	HFE-143a	421-14-7	100.04	248.93	377.92	3.642	180.60	10.5%–21.5% (dry air)	616.0
Methyl pentafluoroethyl ether	HFE-245mc	22410-44-2	150.05	278.78	406.82	2.886	152.64	10.5%–13.5% (dry air)	747.0
2,2,2-Trifluoroethyl difluoromethyl ether	HFE-245mf	1885-48-9	150.05	302.39	444.88	3.428	186.54	Non-flammable	878.0
Hexafluoroisopropyl methyl ether	HFE-356mmz	13171-18-1	182.07	322.43	459.61	2.699	172.13	5.25–15.0% (dry air)	8.1
Heptafluoro-1-methoxypropane	HFE-7000	375-03-1	200.06	307.34	437.66	2.478		Non-flammable	576.0
Methyl Perfluorobutyl Ether	HFE-7100	163702-07-6	250.06	332.65	458.00	2.220	138.95	Non-flammable	490.5
Ethyl Perfluorobutyl Ether	HFE-7200	163702-05-4	264.09	349.25	482.02	1.976	131.82	Non-flammable	34.3
1,1,1,2,2,3,4,5,5,5-Decafluoro-3-methoxy-4-(trifluoromethyl) pentane	HFE-7300	132182-92-4	350.08	375.40	497.00	1.454	133.46	Non-flammable	405.0
3-Ethoxy-1,1,1,2,3,4,4,5,5,6,6,6-dodecafluoro-2-(trifluoromethyl) hexane	HFE-7500	297730-93-9	414.11	412.30	559.00	1.625	111.72	Non-flammable	13.00

[a] Reference [37].
[b] Calculated with the Watson equation with the parameters provided by the NIST TDE [37].
[c] Defined as the lowest and greatest concentrations of a combustible substance capable of producing a flash fire in the presence of an ignition source under specified conditions. References [38–43].
[d] Global Warming Potential. Reference [9].

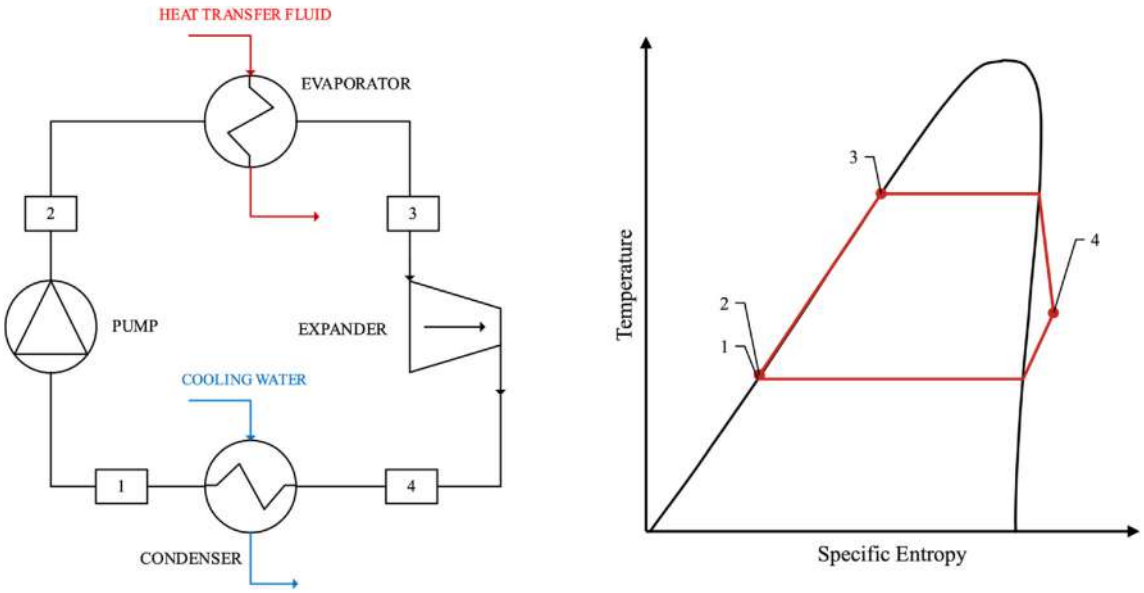

Fig. 1. Schematic diagram of the studied Organic Rankine Cycle (left) and T-S diagram (right).

negligible, and the working fluid efficiencies were supposed to be constant. Also, the volumetric expansion ratio (ER) (i.e., the variation of the working fluid's specific volume during the expansion) was limited to 5 to achieve the scroll expander's maximal isentropic efficiency. Finally, the condenser and evaporator were modeled with a pinch temperature of more than 5 K to ensure proper heat transmission between the two fluids [20,47]. Cooling water (CW) was considered as the cooling fluid at an inlet temperature of 291.15 K and a pressure of 304 kPa. DOWTHERM A, a synthetic organic heat transfer fluid designed for high-temperature heat transfer applications, was chosen as the Heating Fluid (HF) at an inlet temperature of 473.15 K and the same pressure as the cooling fluid.

Overall, the cycle must deliver more than 2 kW of electric power. Isentropic and mechanical efficiencies are assumed to be 65% and 90% for the expander, and 50% and 70% for the pump, respectively. To simplify the model, heat transfer efficiencies were not considered for the condenser and the evaporator. All the performance criteria and constraints are summarized in Table 2.

The main objective of an ORC process is to deliver maximum electricity production with the lowest service fluid consumption (i.e., mass flows of CW and HF required). This is determined, not

Table 2
Performance criteria, constraints, and component efficiencies.

Isentropic efficiency of the expander (%)	65
Mechanical efficiency of the expander (%)	90
Isentropic efficiency of the feed pump (%)	50
Mechanical efficiency of the feed pump (%)	70
HF Inlet temperature (K)	473.15
CW Inlet temperature (K)	291.15
Subcooling temperature (K)	2
Pinch point temperature difference (K)	>5
Volumetric expansion ratio	<5
Inlet pressure for cooling/heating fluids (kPa)	304
Net electric power (kW)	>2

only by the fluid choice, but also by the selected operating conditions. Consequently, a thermodynamic analysis is proposed and fluid properties at each point of the ORC have been calculated based on the aforementioned considerations for steady-state conditions. Under these circumstances, the energy balance at the evaporator can be written as:

$$\dot{m}_{HF} \cdot \left(h_{HF,in} - h_{HF,out}\right) = \dot{m}_{ORC} \cdot (h_3 - h_2) \tag{1}$$

$$h_2 = h_1 + \frac{h_{2,\,isen} - h_1}{\eta_{isen,\,pump}}, \tag{2}$$

where $\dot{m}_{HF}$ and $\dot{m}_{ORC}$ are the mass flows (kg s^{-1}) of the heating and working fluids, respectively, $h_{HF,in}$ and $h_{HF,out}$ are the inlet and outlet evaporator enthalpies (kJ kg^{-1}) of the heating fluid, h_3 and h_2 are the enthalpies of the ORC working fluid at the same points (see Fig. 1), and $\eta_{isen,\,pump}$ is the isentropic efficiency of the pump. Likewise, an equivalent energy balance is calculated for the condenser:

$$\dot{m}_{CW} \cdot \left(h_{CW,\,in} - h_{CW,\,out}\right) = \dot{m}_{ORC} \cdot (h_1 - h_4) \tag{3}$$

$$h_4 = h_3 - \left(h_3 - h_{4,\,isen}\right) \cdot \eta_{isen,\,exp} \tag{4}$$

Therein, $\dot{m}_{CW}$ refers to the mass flow of cooling water (kg s^{-1}) and $h_{CW,\,in}$ and $h_{CW,\,out}$ are the inlet and outlet enthalpies (kJ kg^{-1}) for the CW at the condenser, while $\eta_{isen,\,exp}$ is the isentropic efficiency of the expander.

The net power of the system (kW) (Eq (7)) is obtained from the pump power consumption (Eq (5)) and the power generated by the expander (Eq (6)):

$$W_p = \dot{m}_{ORC} \cdot \frac{(h_2 - h_1)}{\eta_{mec,\,pump}} \tag{5}$$

$$W_{exp} = \dot{m}_{ORC} \cdot (h_3 - h_4) \cdot \eta_{mec,\,exp} \tag{6}$$

$$W_{net} = W_p - W_{exp} \tag{7}$$

Where $\eta_{mec,\,pump}$ and $\eta_{mec,\,exp}$ are the mechanical efficiencies of the pump and the expander, respectively.

Finally, the thermal efficiency (Eq (8)) indicates the amount of energy received by the working fluid in the evaporator that is converted into net work produced:

$$\eta_{ORC} = \frac{W_{exp} - W_p}{Q_{evap}} \tag{8}$$

$$Q_{evap} = \dot{m}_{ORC} \cdot (h_3 - h_2) \tag{9}$$

The cycle's energy balances are solved iteratively, with the evaporation and condensation temperatures (T_3 and T_4, respectively) and the working fluid, heating fluid, and cooling water flow rates as manipulated variables.

An Aspen Plus (v.12.1) model of the ORC proposed has been used to determine the operating conditions for each fluid, following the iterative scheme depicted in Fig. 2. The physicochemical thermodynamic properties at the conditions resulting from this evaluation are calculated using polar soft-SAFT. First, the evaporating temperature (T_3) is set by imposing a value that provides a difference with the inlet heating fluid temperature of at least 5 K, with a maximum value of 90% of the working fluid's critical temperature. This additional restriction is established to avoid errors in the calculation of the fluid properties with polar soft-SAFT, which, as other mean-field theories, overestimates the calculations near the critical region. Once T_3 is fixed, the cycle's maximum pressure, P_2, is automatically obtained, as it equals the vapor saturation pressure at T_3 (no head losses in the condenser or the evaporator have been considered). Likewise, a condensation temperature (T_4) is given under the constraint of the volumetric ER criteria, which must be below 5. Analogously, the minimum cycle's pressure, P_4, is calculated as the liquid's saturation pressure at T_4 and must not be lower than atmospheric pressure [20]. Next, the value of the mass flow rate of the working fluid is iterated until it satisfies the net electrical power set out in Table 2. Finally, the flow rates of the heating and cooling service fluids are determined by iteratively solving the energy balances in the condenser and evaporator, under the constraint that the calculated output fluid temperatures must not go below the pinch point.

3. Thermophysical characterization of HFE

3.1. Polar Soft-SAFT EoS

The soft-SAFT EoS is one of the most successful versions of the original Statistical Association Fluid Theory [48]. Soft-SAFT provides a theoretical framework where the compounds are modeled as coarse-grained molecules and the key physical molecular interactions are accounted through the calculation of the residual Helmholtz energy of the system using statistical mechanics. Indeed, molecular structure in terms of chain length and segment diameter, van der Waals and hydrogen bonding interactions, and polarity are included in the equation (Eq (10)) as a sum of independent contributions based on a reference term, (A^{ref}), which is a Lennard-Jones (LJ) sphere in the case of soft-SAFT.

$$A^{res} = A - A^{id} = A^{ref} + A^{chain} + A^{assoc} + A^{polar} \tag{10}$$

A^{ref} contains the repulsive and dispersive interactions between individual monomers of the LJ reference. The chain and association terms (A^{chain} and A^{assoc}, respectively) involve structural information to evaluate the contribution of the formation of chains, based on the connectivity of the individual LJ spheres, as well as the impact of hydrogen bonding, which considers highly directional and short-range interactions. In the soft-SAFT version used in this work, a polar term (A^{polar}) is included to account for dipole effects. This term is based on the multipolar expression originally proposed by Twu and Gubbins [49,50] and later extended by Jog and Chapman [51] to chain molecules, written as a Padé approximation [52]:

$$A^{polar} \approx \frac{a_2}{1 - \frac{a_3}{a_2}} \tag{11}$$

a_2 and a_3 are the second and third-order terms in the perturbation expansion and are taken from the interpolation equations over

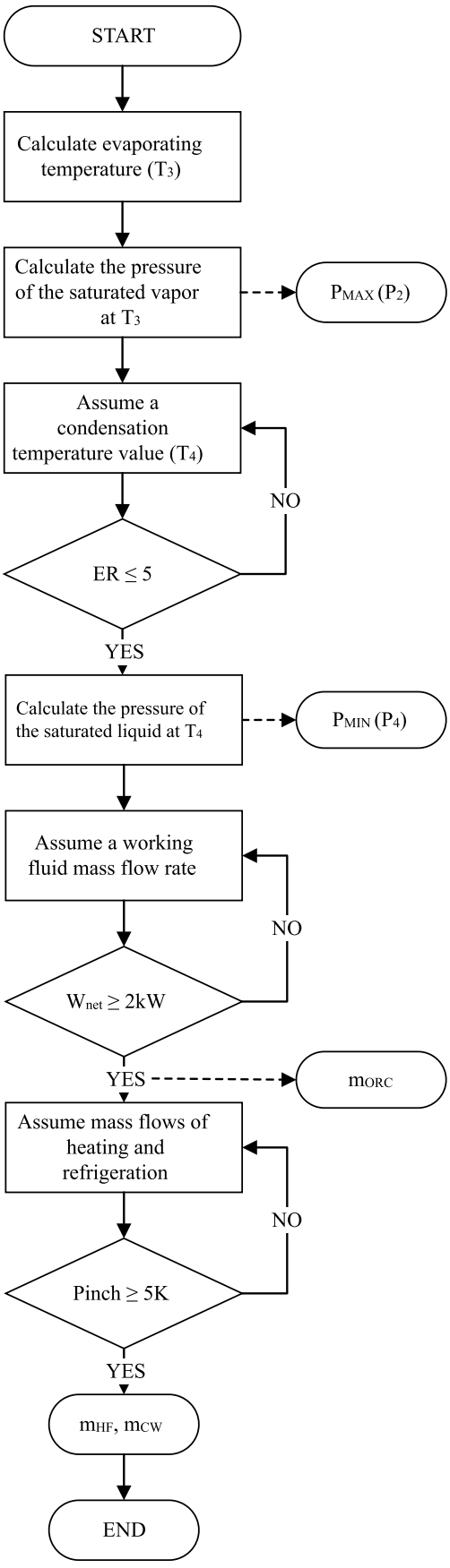

Fig. 2. *ORC* calculation algorithm.

pair- and triplet-correlation functions of a LJ fluid proposed by Luckas et al. [53]. Further details on the original soft-SAFT [23], as well as the addition of the polar treatment [36], can be found in detail in previous literature.

Eq (10) describes each fluid of interest through a careful parametrization, given by key physical parameters, which are seen as compound descriptors. Hence, benchmark HFC-245fa and all HFEs are represented as homonuclear non-associating LJ chainlike fluids in the polar soft-SAFT framework, explicitly considering their dipole moment caused by the electronegative fluorine and oxygen, and their asymmetric molecular structure, which is a key feature affecting its thermodynamic properties. For these fluids, the association contribution, A^{assoc}, has been omitted in an effort to avoid an over-parametrization that would not represent the key physical interactions occurring in those molecules, based on the fact that polar interactions are dominant. Consequently, a total of five molecular parameters are used to describe these molecules: the LJ segment diameter (σ_i), the chain length (m_i), the LJ segments dispersive energy (ε_i), the dipole moment (μ) and the fraction of segments affected by the polar moment (x_p).

As it will be shown in the next section, further validation of the parametrization is carried out by studying binary mixtures with some additional compounds, such as ethers and alcohols. Hence, an adequate molecular model must also be proposed for these molecules. Acetone and ethyl acetate follow the same pattern as HFEs, being modeled as homonuclear chains with specific dipole moments. However, hydrogen bonding interactions are dominant in alcohols due to the presence of a hydroxyl group and cannot be omitted. In this work, methanol and 1-propanol are modeled, for the first time, using a combination of dipole + association terms to consider both, the permanent dipolar and hydrogen bonding interactions, adding two additional parameters, ε^{HB} for the square-well energy parameter of an association site, and κ^{HB} for the volume of association, to the parametrization of these specific compounds.

Dipole moments, μ, for HFE-143a, HFE-245mf, HFE-245mc, HFE-7000, HFE-7100, acetone, ethyl acetate, methanol, and 1-propanol were retrieved from Aspen Plus Database v.12.1. For the remaining ones, DFT (Density Functional Theory) calculations were employed for their estimation. Optimized structures were generated with TmoleX software v.21.0.1 [54] at the gas phase using the triple-ζ valence potential (def-TZVP) basis with the Becke and Perdew (BP) functional using the resolution of identity (RI) approximation and a convergence criterion of 10^{-6} Hartree. Next, a second optimization was performed using the TZVDP-FINE level, a more computationally-demanding level considered the *best quality* calculation method currently available [55]. Density functionals have been reported to be quite good at predicting dipole moments, with low Root Mean Squared errors compared to the reference values [56].

The rest of the polar soft-SAFT molecular parameters, m, σ, ε, and x_P (as well as κ^{HB} and ε^{HB} for the alcohols) were fitted to the available experimental saturated liquid density and vapor pressure data. A careful analysis of the values obtained and how they are related to the structural features of these compounds is given in Section 3.2.

Finally, surface tension calculations were also performed through the use of the density gradient theory (DGT) [57], stemming from the van der Waals theory for inhomogeneous fluids [58], and coupled into the polar soft-SAFT EoS. The Helmholtz free energy is provided as a function of the density to the space coordinates, based on the assumption that the density gradient is slight compared to the reciprocal value of the intermolecular distance, thus allowing to treat the density and its derivatives as

independent variables. With this, the interfacial tension of a planar interface can be computed with Eq (12):

$$\gamma = \sum_i \sum_j \int_{-\infty}^{\infty} c_{ij} \frac{d\rho_i}{dz} \frac{d\rho_j}{dz} dz, \tag{12}$$

where $d\rho_i$ and $d\rho_j$ are the density profiles of the molecules i and j across the interface. An influence parameter, c_{ij}, is defined and treated phenomenologically as a parameter fitted to experimental surface tension data. Further details on the implementation of the theory can be obtained in the works of Mejía et al. [59], Vilaseca et al. [60] and Pàmies [61].

3.2. Molecular modeling and parametrization analysis

As a preliminary step prior to the drop-in assessment, it is necessary to adequately characterize the thermophysical behavior of the investigated HFEs in the range of temperature and saturation conditions found in ORCs. In this regard, the polar soft-SAFT EoS is an excellent platform due to its versatility and predictive capabilities, rooted in an adequate picture, in terms of molecular model, of the compounds studied.

The optimized polar soft-SAFT molecular parameters for the nine studied HFEs, as well as the average deviations obtained from the experimental saturated liquid density (AAD_D) and vapor pressure (AAD_P), are presented in Table 3.

The physical meaning of these parameters, which is related to the size and energy of the molecule, allows for the extraction of molecular features and comprehension of their impact on macro-level properties. It can be noticed that the volume of the molecule, reproduced by $m\sigma^3$, increases with the size of the refrigerant. However, this increase cannot be strictly related to the carbon chain length (a common approach done for other families, such as n-alkanes or 1-alkanols [71]) due to the influence of the number and position of fluorine atoms located in the molecule. For this reason, a direct relation between the m chain length parameter and the number of carbons cannot be correlated [31], being the $m\sigma^3$ volume comparison a more appropriate descriptor [30].

Another relevant aspect is the existing correlation between the effective dipole (expressed as the dipole moment value multiplied by the fraction of the molecule affected by this dipole, x_p) and the segment diameter, σ. This is appreciated in Table 3 and, visually, in Fig. 3. The polar effect is clearly influenced by the presence of fluorine atoms connected to the main carbon chain, described with SAFT through a higher diameter. Indeed, the size of the filled circles in Fig. 3 indicates the number of fluorine atoms in each molecule. Still, some discrepancies are observed as a consequence of the exact

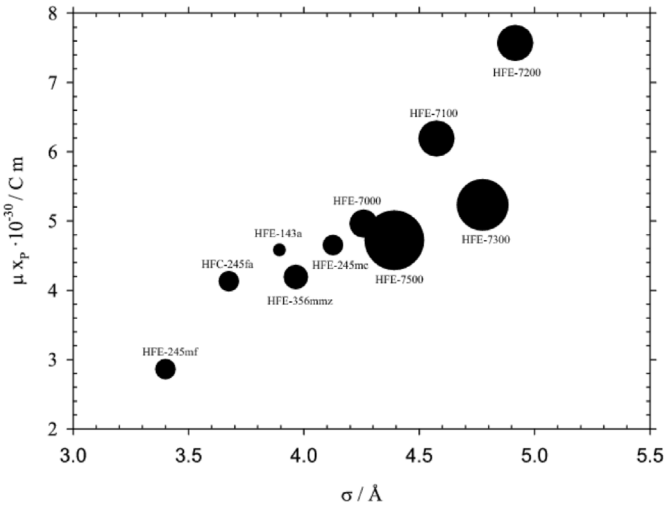

Fig. 3. Effect of the product of the dipole moment. μ, and the polar fraction of the molecule on the segment diameter σ. Note that the size of the symbols reflects the number of fluorine atoms in the molecule.

location of these atoms. For example, HFE-143a contains only 3 F-atoms, but located in one specific side of the molecule, increasing the asymmetry and the polarity (as shown in the σ-surface diagrams in Fig. 4). Contrarily, HFE-7500 has 15 F-atoms, but quite symmetrically distributed along the molecule, resulting in a more electroneutral molecule compared to other HFEs of the 7000-series.

To further understand the significance of explicitly accounting for the polarity of the refrigerants explored herein, the relative contribution of the different terms (Reference, Chain, and Polar) to the residual Helmholtz free energy (Eq (10)) was calculated at saturated liquid conditions for all fluids at T = 273.15 K. Note that the ideal contribution has also been estimated, and proven to be dominant at the established conditions, but has not been included in the figure for a better appreciation of the polarity effect among the residual terms. The results, displayed in Fig. 5, reveal that the polar term has a significant impact in all the compounds, with contributions ranging from 27% to 53%, except for HFE-7300 (16%), differing from a recent publication carried out with PC-SAFT [21]. It can be seen that, for fluids with equivalent degrees of fluorination (HFE-356mmz vs. HFE-7100, HFE-143a vs. HFE-245mf/mc, or HFE-7200 vs. HFE-7300), the polar contribution diminishes as the carbon chain increases. This can be associated with a more symmetrical charge distribution, as observed from the COSMO σ-surface diagrams in Fig. 4. In any case, it is clear that the polar term will

Table 3
Optimized polar soft-SAFT Molecular parameters for the working fluids investigated in this work.

Compound	**m**	**σ**(A)	**ε/k$_B$(K)**	**μ × 10^{-30}(Cm)**	**x$_P$**	**AAD$_P$** (%)[a]	**AAD$_D$** (%)[b]
HFC-245fa[c]	2.479	3.675	197.1	5.166	0.800	1.593	0.596
HFE-143a	1.784	3.894	167.9	8.333	0.550	1.541	1.254
HFE-245mf	3.309	3.400	179.6	5.440	0.525	5.568	1.172
HFE-245mc	2.051	4.126	179.0	9.290	0.500	1.938	0.462
HFE-356mmz	2.681	3.965	175.4	9.856	0.425	1.585	0.822
HFE-7000	2.324	4.259	181.3	9.910	0.500	1.739	0.505
HFE-7100	2.283	4.575	204.9	9.900	0.625	2.696	0.166
HFE-7200	2.113	4.916	214.6	11.21	0.675	3.243	0.162
HFE-7300	2.636	4.775	250.6	8.049	0.650	4.035	0.030
HFE-7500	3.940	4.392	198.3	9.435	0.500	5.659	2.729

[a] Experimental vapor pressure from refs. [39–43,62–68].
[b] Experimental saturated densities from refs. [63,64,67,69,70].
[c] Molecular parameters retrieved from [30].

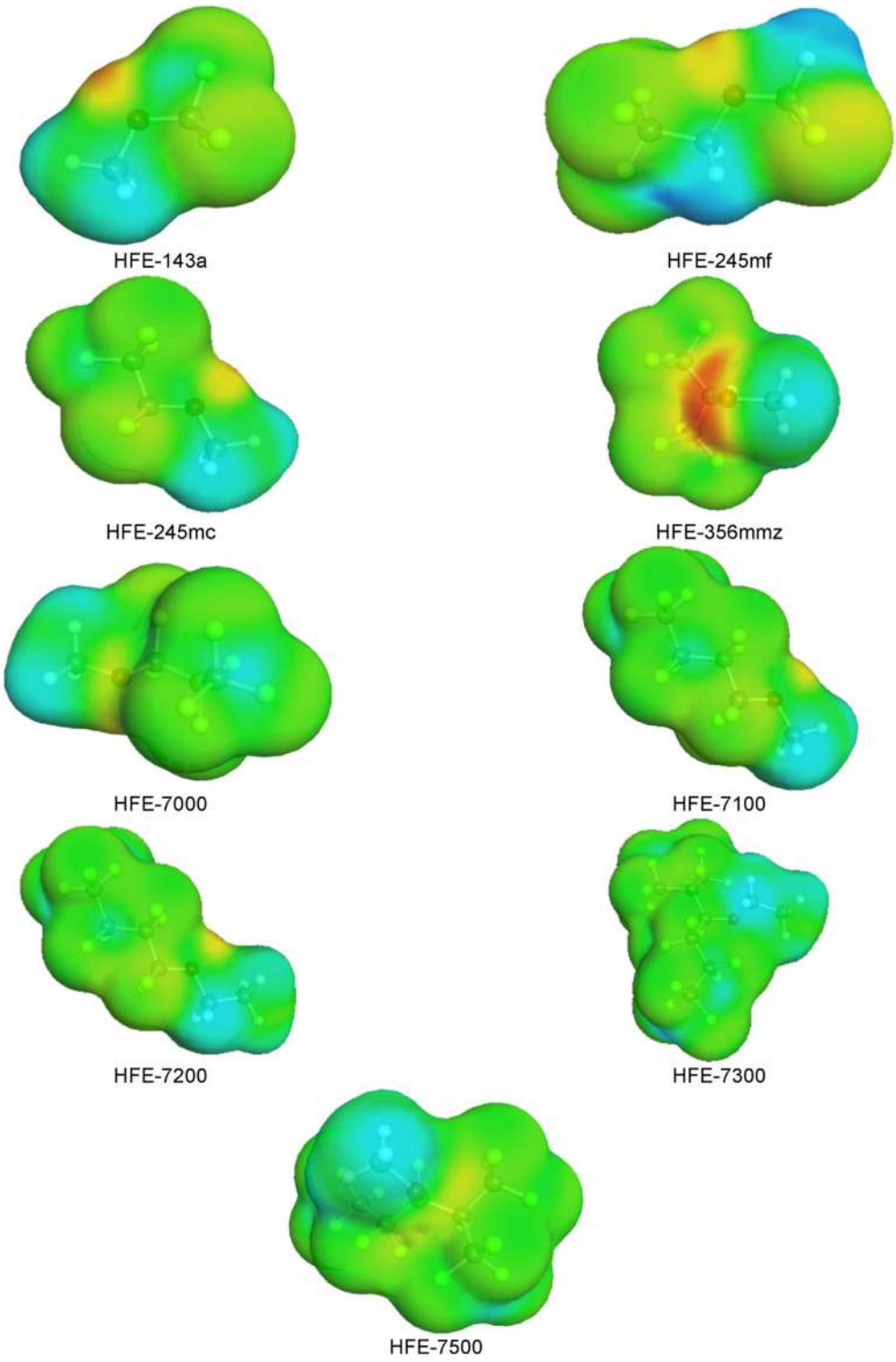

Fig. 4. Sigma surfaces for the HFEs investigated in this work predicted by conductor-like screening model for real solvents (COSMO-RS) analysis. Green zones reveal non-polar regions, blue regions show H-bond donors (electropositive area) and red regions depict H-bond acceptors (electronegative area).

affect the thermodynamic properties, such as vapor pressure or enthalpy of vaporization, although it is difficult to separate this explicit effect from the rest of contributions, since all of them are interrelated [30].

3.3. Thermodynamic characterization of HFEs

The parameters presented can accurately reproduce the phase equilibria diagrams of all fluids, as provided in Fig. 6 for the vapor pressure (top) and the saturated vapor-liquid densities (bottom). The average absolute deviation (AAD) for the vapor pressure is below 2% in most cases, with the exceptions of HFE-245mf, HFE-

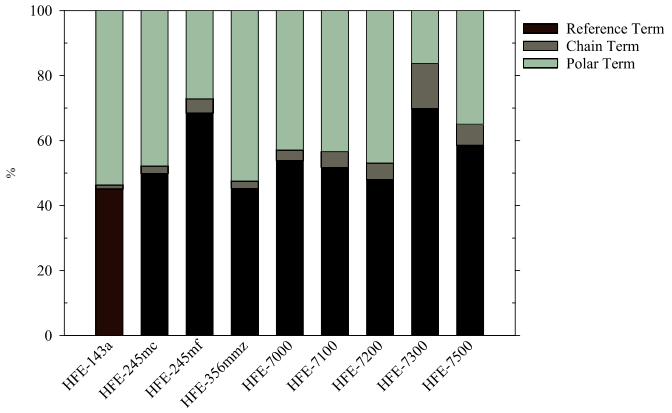

Fig. 5. Relative term contributions to the residual Helmholtz energy predicted with polar soft-SAFT at T = 273.15K and saturation conditions for the liquid phase of the HFEs characterized in this work.

7100 and HFE-7500, still in an acceptable range between 2.5 and 6%. The comparison of the vapor pressures reveals that HFE-245mc and HFE-143a can achieve higher evaporation temperatures than HFC-245fa at the same conditions, which is expected to improve the cycle thermal efficiency [3]. Similar behavior is observed for HFE-245mf, HFE-7000, and HFE-356mmz at moderate working pressures. Finally, high molecular weight HFEs, such as HFE-7500 and HFE-7300, exhibit lower saturation pressures and high normal boiling points, being a clear disadvantage when choosing an ORC working fluid, since it is necessary to increase the temperature to avoid working under atmospheric pressure, with a negative impact on the thermal efficiency. The results are consistent with the vaporization enthalpies shown in Table 1, where these components have the lowest values.

The saturated liquid density is even better described, as shown in Fig. 6 bottom, with an AAD below 1% with the exception of HFE-245mf and HFE-7500, both below 3%. Interestingly, vapor densities

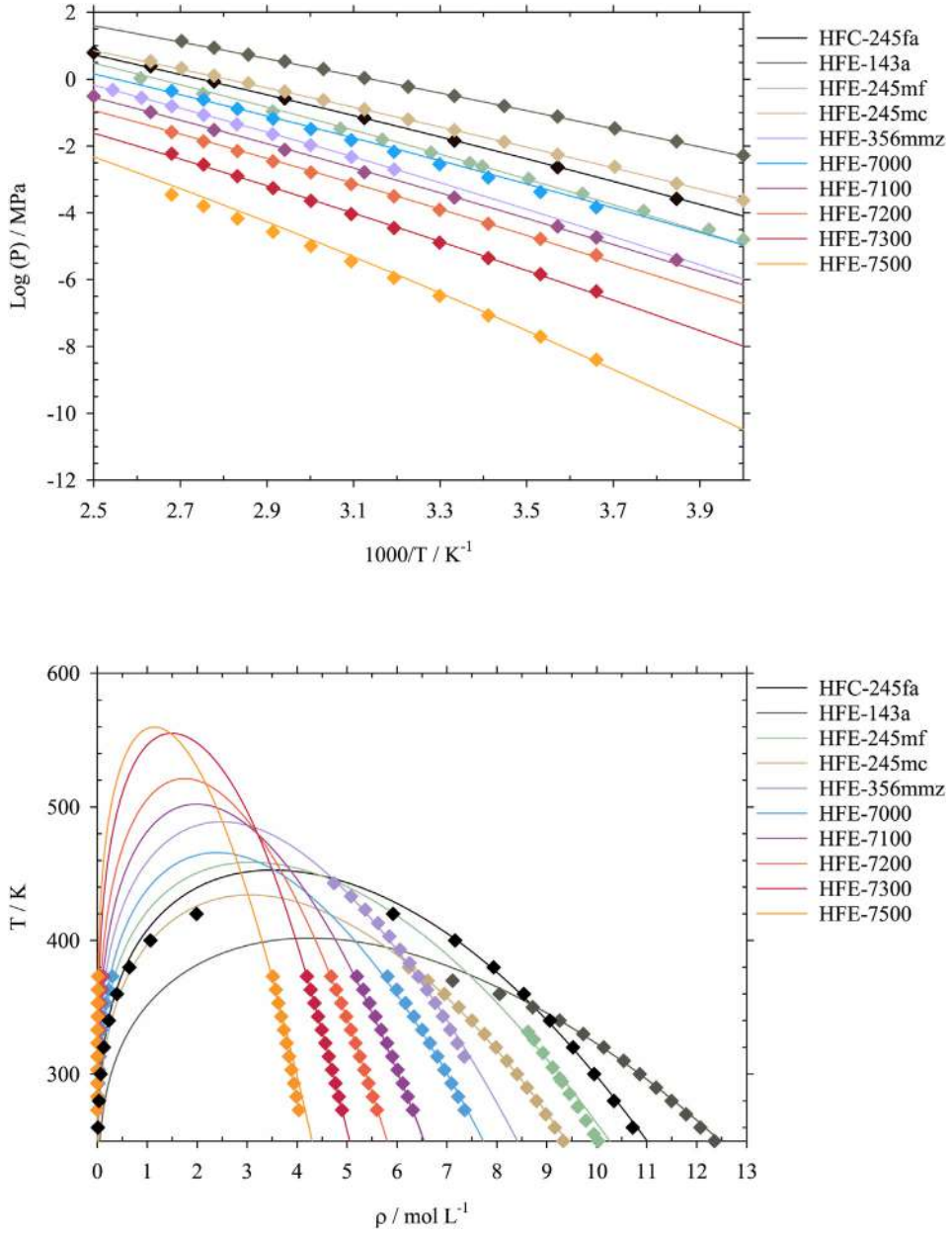

Fig. 6. Vapor pressures (top) and coexisting densities (bottom) for the working fluids studied in this work. Symbols represent the experimental data (see references in Table 3) and solid lines are the polar soft-SAFT calculations.

are also predicted in very good agreement with the available experimental information. Coexistence densities also play an essential role, particularly in the sizing of the equipment [4,72]; although the functional design of the ORC is beyond the scope of this work, the behavior is comparable to what has previously been observed for the vapor pressures: HFE-245mc and HFE-143a exhibit higher vapor densities, leading to lower volume flow rates at equal mass flow. This would eventually reduce the cost of the system as the size of the heat exchangers would not have to be increased to limit the pressure drops, as it occurs in low-vapor density fluids with high volume flow rates [72].

The thermodynamic characterization of pure HFEs has been completed by calculating the surface tension of the fluids for which experimental data are available [63]. The results are shown in Fig. 7. Even if the influence parameter c is adjusted to data, as indicated in Section 3.1, the correct description of the slope of the surface tension can only be achieved if the right balance between the van der Waals and the polar forces is given. The description of the surface tension is, in all cases, excellent using a temperature independent influence parameter (AAD lower than 2.6%, see Table 4), corroborating the validity of the molecular parameters presented in Table 3.

Further validation of the adequacy of the selected molecular parameters, as well as the impact of the polar contribution in those compounds, is provided by describing the phase behavior of binary systems with other molecules. Reported experimental data of alcohols or acetates are commonly encountered in binary combinations with HFEs, as these mixtures are present in advanced cleaning solvents [73,74]. Fig. 8 shows the VLE of HFE-7000, HFE-7100, and HFE-356mmz with solvents such as acetone, methanol, ethyl acetate, or 1-propanol, whose molecular parameters are presented in Table 5. In all cases, a very good representation of the nonideal behavior of these mixtures is achieved, with only some slight deviations for the HFE-356mmz + methanol at the azeotropic concentration. These results are obtained by using a single energy binary parameter (ξ), described as $\varepsilon_{ij} = \xi\sqrt{\varepsilon_{ii}\varepsilon_{jj}}$, to quantitatively fit the experimental data. However, a closer examination of ξ indicates that they are all close to unity. It is important to notice that a value of one means that the system is predicted using the combining rules without any additional correction. While the use of this parameter is typically required to account for structural differences among molecules, the inclusion of the polar-polar contributions allows to decrease this degree of correction. Here, a pure prediction ($\xi = 1$), not shown for clarity, is even capable to qualitatively reproduce the different azeotropes and complex behavior in all systems. Additional binary mixture combinations between HFEs and these compounds exhibit very similar behavior (see Figure S1 from Supplementary data).

Table 4
Optimized influence parameter (c) for the 3M's Novec engineered fluids and its deviation from experimental values [63].

Compound	$\mathbf{c} \times 10^{-18}$ (J m^5 mol^{-2})	$\mathbf{AAD_{ST}}$ (%)
HFE-7000	0.3259	1.654
HFE-7100	0.4661	2.520
HFE-7200	0.6637	1.519
HFE-7300	0.8418	1.024
HFE-7500	1.220	2.509

4. ORC drop-in assessment results

Once the parametrization of HFEs has been validated, saturated mass entropies and enthalpies have been predicted using the same set of parameters (Table 3), as this is a key information so as to assess their adequacy in ORCs. While the residual term has been predicted with polar soft-SAFT, the ideal term has been obtained from the Aspen Properties database, using the REFPROP propery package included in version 12.1. Enthalpy and entropy values are referenced to 200 kJ kg^{-1} and 1 kJ kg^{-1} K^{-1} respectively for saturated liquid at 273.15 K. A summary of the results for some of the most promising working fluids is represented in Fig. 9, while the remaining ones are included in Figure S2 from the Supplementary data. The results reveal that all the studied compounds exhibit, either a near-zero or a positive slope (dS/dT) in the vapor saturation curve, indicating a near-isentropic (HFC-245fa and HFE-143a) or a dry (HFE-7000 or HFE-7100) fluid behavior, respectively. Both behaviors are recommended for ORC applications, since no superheating is required to avoid condensation during the isentropic expansion [6,79]. Indeed, it is even possible to predict the transition from wet to dry fluids as a function of the operating conditions chosen using SAFT approaches [80,81], although this is out of the

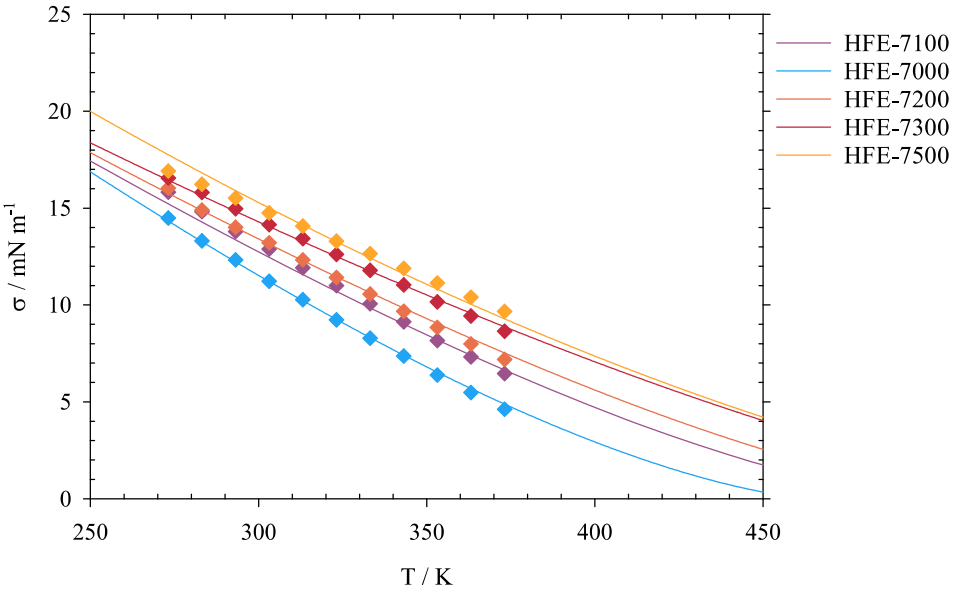

Fig. 7. Surface tensions for some of the hydrofluoroethers studied in this work. Symbols represent the experimental data [63] and solid lines are the soft-SAFT calculations.

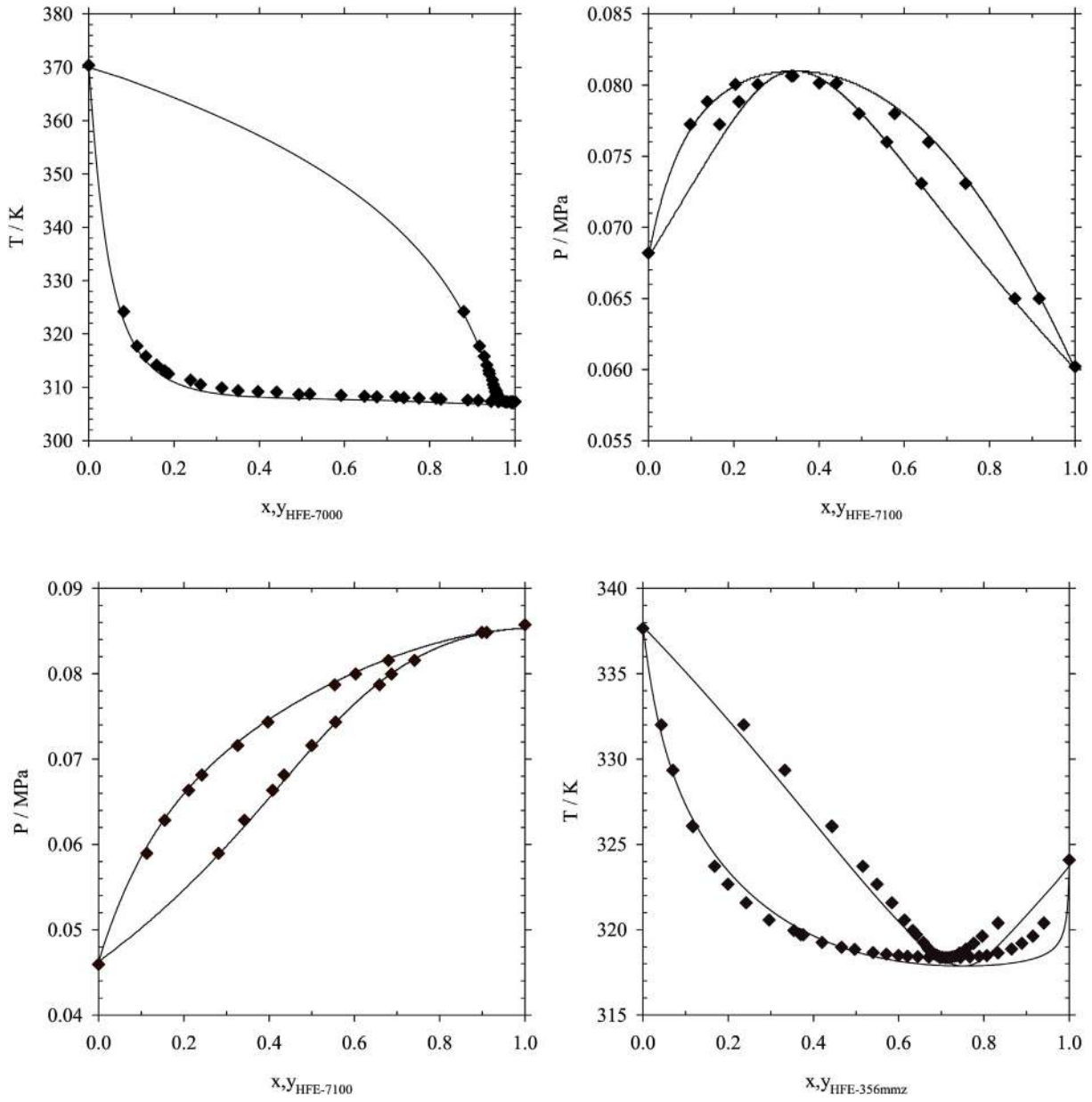

Fig. 8. Binary VLE for HFE-7000 + 1-propanol (top-left), HFE-7100 + Acetone (top-right) and Ethyl Acetate (bottom-left), and HFE-356mmz + Methanol (bottom-right). Symbols represent the experimental data [76–78] and solid lines are the polar soft-SAFT calculations. Isotherm plots are performed at 318.15K (top-right) and at 328.15K (bottom-left), and isobaric plots are both at 0.1013 MPa. One binary parameter (ξ) was used for the fitting, with values of 1.005 (top-left), 0.986 (top-right), 0.990 (bottom-left) and 1.070 (bottom-right).

Table 5
Optimized polar soft-SAFT molecular parameters for selected alcohols and ethers.

Compound	**m**	**σ**(A)	**ε/k$_B$**(**K**)	**ε^{HB}/k$_B$** (K)	**κ^{HB}**(Å^3)	**μ × 10^{-30}**(**Cm**)	**x$_P$**	**AAD$_P$** (%)	**AAD$_D$** (%)
Acetone[a]	1.849	3.827	275.70	n.a	n.a	9.610	0.333	1.640	0.910
Methanol	1.123	3.748	214.31	3436	4099	5.504	0.350	1.088	0.492
Ethyl Acetate	2.797	3.620	247.16	n.a	n.a	5.940	0.475	1.687	0.615
1-propanol	1.981	3.826	263.04	3249	2250	5.600	0.338	1.128	0.312

[a] Molecular parameters retrieved from [75].

scope of this work. The predictions obtained with the soft-SAFT models are in agreement with the REFPROP correlations for the fluids for which data are available. The major deviations are noticed in the high temperature range of the vapor phase, particularly for the base case (HFC-245fa). This is caused by the overprediction of the critical point, a common drawback of SAFT mean field approaches. It is important to note that HFC-245fa parameters were transferred from a previous work [30], in which the molecular

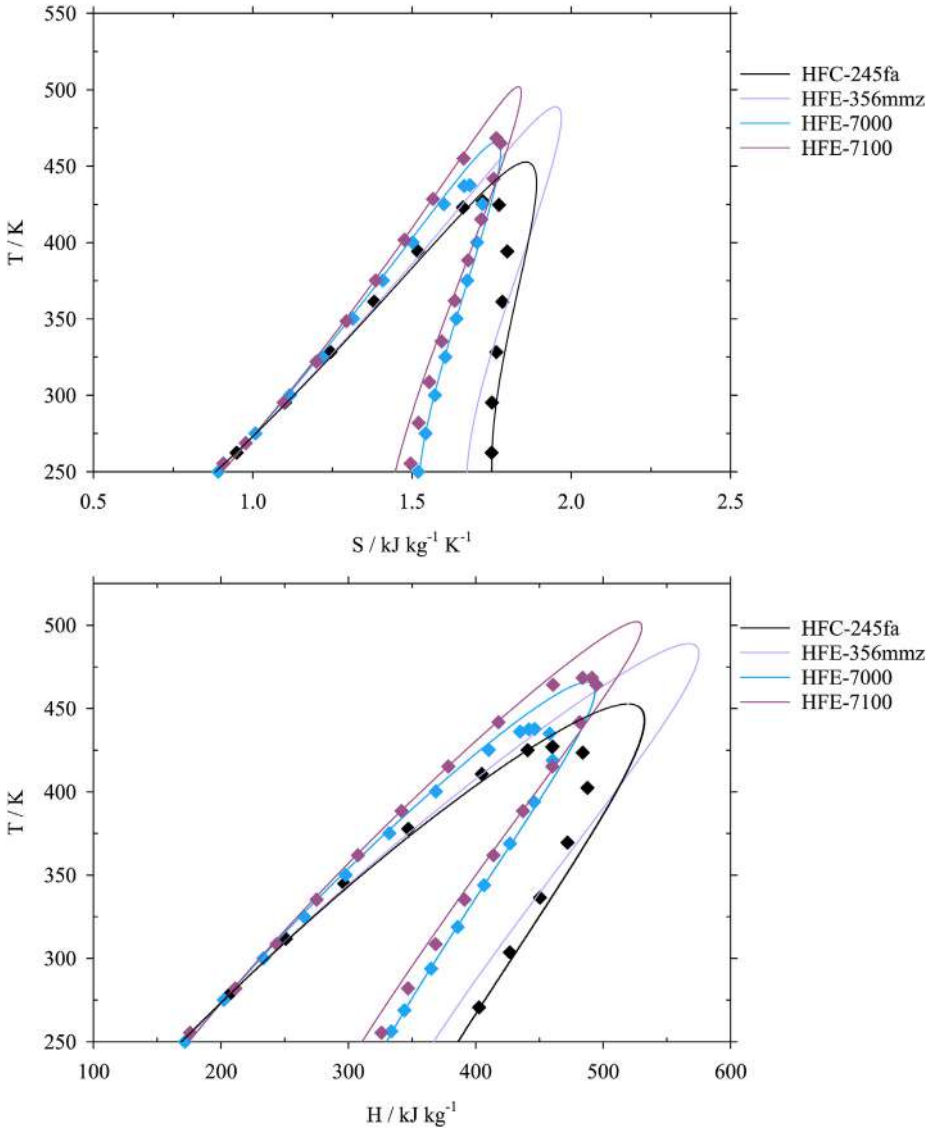

Fig. 9. Saturated mass entropies (top) and enthapies (bottom) for a selection of working fluids studied in this work. Symbols represent the calculations by REFPROP [64] and solid lines are the polar soft-SAFT EoS.

parameters had been fitted to a lower temperature range. While it is possible to reduce these deviations by reparametrizing this compound at a higher temperature range, the authors have preferred to maintain these parameters for consistency, given the marginal improvement that would be achieved. In any case, and as shown in previous section, the soft-SAFT characterization ensures a good description in the range of temperature and pressure of the ORC working conditions.

Next, the information gathered for all HFEs, along with the benchmark HFC, is used to optimize the ORC represented in Fig. 1, based on the choice of several Key Performance Indicators (KPIs). These include the cycle thermal efficiency (η_{ORC}), as defined by Eq (8), and the service fluids (i.e. CW, and HF) and working fluid mass flow rates. The choice is based on the search for reducing the energy inputs coming from the mass flows, while η_{ORC} is typically seen as an ORC system's performance metric [3]. The main results of the optimization are reported in Table S1 of the Supplementary data.

Fixing a constant net work output, the calculated η_{ORC} for all fluids is given in Fig. 10.

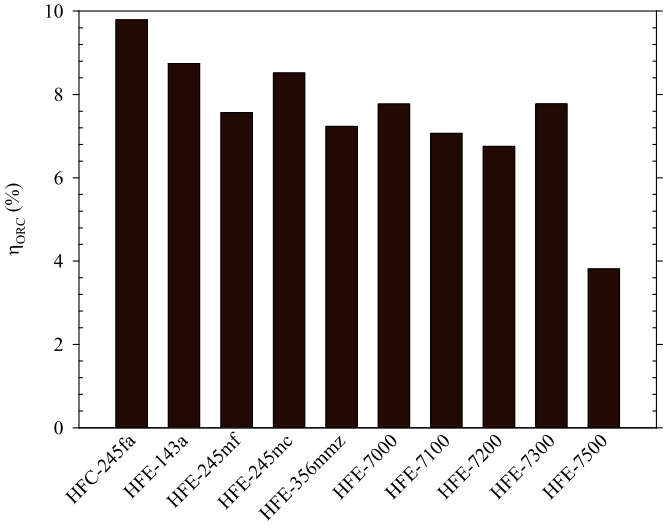

Fig. 10. Cycle thermal efficiencies for the studied working fluids.

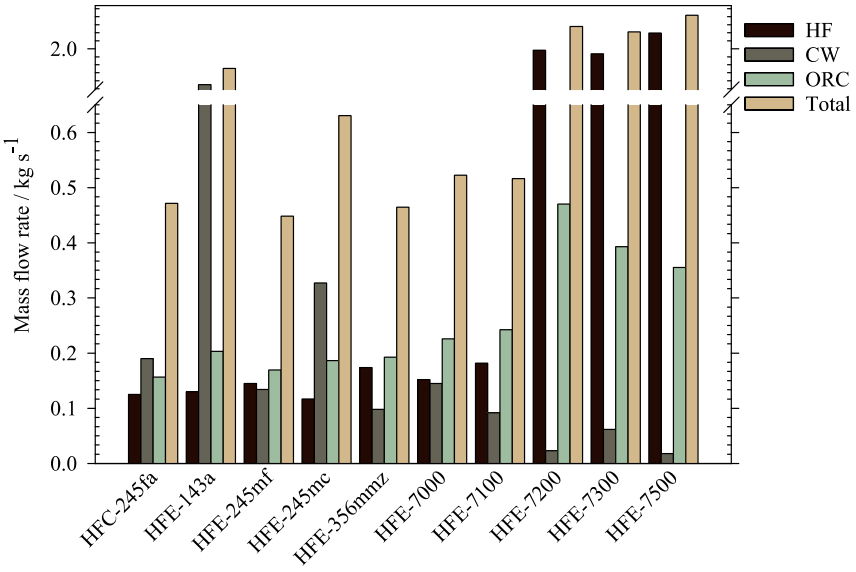

Fig. 11. ORC mass flowrate comparison for the selected working fluids.

While the benchmark HFC-245fa shows the greatest performance (9.80%), the low molecular weight compounds, HFE-143a and HFE-245mc, exhibit cycle yields that are comparable to the reference (8.74% and 8.52%, respectively). This is because, as stated in section 3.3, these fluids have thermodynamic properties that make them suitable for use in ORCs, such as a high vapor pressure or vaporization enthalpy. Nonetheless, with the exception of HFE-7500, no significant changes in the cycle efficiency are seen across the different HFE working fluids provided in this study at the established conditions. This exception is justified since this compound has a lower vapor pressure and a much greater boiling point values than the other fluids evaluated, resulting in a worse performance when compared to the other options.

A comparison between the soft-SAFT predicted efficiencies and those estimated in previous bibliography for some specific compounds (i.e. HFC-245fa, HFE-7000 and HFE-7100) reveal slightly higher values than those of Jang and Lee [20] (4–5%), slightly lower values than the results of Wang et al. [18] (12–13%) and similar results to the molecular dynamic simulations done by Petr and Raabe [6] (7.5%). This comparison must be taken with care, as the methodologies adopted by the different authors differ from each other, as well as the performance constraints and component efficiencies (different evaporation temperature, mass flows, or condensing temperatures). In any case, the results presented in this work fall within the range of expected values and do not prevent the qualitative comparison presented in this section.

Fig. 11 compares the required cooling, heating and working fluid mass flow rates for all the studied cases at the constraint imposed.

In contrast to the results obtained for thermal efficiencies, evident differences are found among all cases. The first evident conclusion is the low suitability of high molecular weight HFE-7200, HFE-7300 and, again, HFE-7500 to become alternative substitutes to HFC-245fa due to their high demand for the heating fluid and working fluid flow rates. This is again related to their high boiling point and low enthalpy of vaporization. Although this facilitates a low CW demand at moderate pressure conditions, they require a higher heat demand to produce 2 kW of electricity and, consequently, a higher flow rate of working fluid and HF.

At the other end of the scale, and despite being the top-performing fluids in terms of thermal efficiency, the low molecular weight HFE-143a and, to a lesser extent, HFE-245mc, also have a severe energy penalty in terms of service fluids needs. In this case, they have the lowest boiling points and, therefore, require a higher cooling water flow rate because they exhibit the lowest condensation temperatures, regardless of having a latent heat very close to the benchmark working fluid.

The remaining fluids present a balanced amount of mass flow rates, which are similar to the HFC-245fa benchmark case. At this stage, it is also important to include the GWP criteria in the selection. While all the fluids evaluated in this work have lower GWPs than the benchmark, HFE-245mf represents a minor decrement and, as far as it does not show a clear improvement, is also discarded at this stage.

According to the findings of this investigation, HFE-7000, HFE-7100, and HFE-356mmz are the best alternatives in single stage ORCs with low-temperature heat sources in terms of thermal efficiency and service fluids consumption. This conclusion partially agrees with the suggestion of Jang and Lee [20], who also recommended the first two options to build a cycle with minimal cooling water usage and moderate maximum pressures, allowing for cost reductions in electricity production. Among the three possibilities, HFE-7000 provides the highest thermal efficiency, while HFE-356mmz requires lower mass flow rates. Again, a key factor to consider is the GWP reduction compared to HFC-245a. While HFE-7000 and HFE-7100 reduce the GWP by 40.12% and 49.06%, respectively, HFE-356mmz provides an astonishing 99.15% reduction. Consequently, the latest one represents one of the most promising choices for the future.

Despite all these facts, it is important to keep in mind that the obtained cycle thermal efficiency is lower than that of HFC-245fa, as it is shown in Fig. 10, due to lower vaporization enthalpies, vapor pressures and critical pressures compared to the benchmark HFC. Indeed, none of the alternatives reaches the same efficiency. This is a clear sign that further improvements will be necessary, undoubtedly pushing this analysis towards the study of working fluid mixtures.

5. Conclusions

In this work, the suitability of nine HFEs as potential working fuids' replacement for HFC-245fa in low-grade waste heat recovery ORCs has been assessed proposing a study based on different key

performance indicators (KPIs) related to energy efficiency. For this purpose, a whole thermodynamic analysis and process performance has been carried out using the polar version of the soft-SAFT molecular-based equation of state. A solid and robust model has been built with the explicit inclusion of the polar interactions present in such fluids, which have proven to have a strong impact in their physicochemical behavior. The proposed model has been used to describe the saturated vapor and liquid densities, vapor pressure, surface tension, mass-enthalpy and mass-entropy diagrams. The model's physical foundation allows for the investigation of the molecular properties of the suggested working fluids and their impact on the physicochemical properties influencing their technical efficiency.

Following this characterization, the suitability of the fluids in an ORC simulated to generate 2 kW of electricity has been evaluated. Apart from the thermal efficiency of the cycle, special consideration has been given to the cooling water, heating fluid and working fluid's flow rates as key performance indicators related to the energy requirements of the system. The results have shown a similar performance in terms of efficiency for all the studied fluids at the process conditions considered (with the exception of HFE-7500), lower in all cases than the benchmark HFC-245fa. However, significant differences have been detected in the required service fluids flow rates. High molecular weight working fluids, such as HFE-7200, HFE-7300, and HFE-7500, have been excluded as suitable alternatives due to their elevated normal boiling points and low vaporization enthalpy, being incompatible with the ORC studied in this work, as they demand large amounts of working and heating fluids. Low molecular weight HFE-143a and HFE-245mc suffer a substantial energy penalty in terms of cooling water demands, as a consequence of their low boiling points. HFE-245mf is discarded at a final stage since it has a high GWP value, representing a minor decrease compared to the benchmark case. HFE-356mmz, HFE-7000 and HFE-7100 are considered as possible replacements for HFC-245fa in a simple ORC design, with the first two having the best environmental (HFE-356mmz) and technical (HFE-7000) performance. Still, their lower thermal efficiencies compared to the benchmark working fluid suggest that none of the proposed candidates is a direct improvement over HFC-245fa. Nonetheless, the consistent and robust methodology described here can be easily extended to the evaluation of mixtures, either between HFEs and HFOs, or even mixed with intermediate GWP 3rd generation refrigerants, facilitating the pre-design of novel and improved working fluids.

Credit author statement

Daniel Jovell: Conceptualization, Methodology, Validation, Investigation, Writing – original draft. **Rafael Gonzalez-Olmos**: Investigation, Writing – review & editing, Funding acquisition. **Fèlix Llovell**: Conceptualization, Investigation, Writing – review & editing, Funding acquisition, Supervision.

Declaration of competing interest

The authors declare that they have no known competing financial interests or personal relationships that could have appeared to influence the work reported in this paper.

Acknowledgments

This research is supported by project STOP-F-Gas (PID2019-108014RB-C21) funded by the Spanish Ministry of Science and Innovation. GESPA group has been recognized as Consolidated Research Group by the Catalan Government (2017-SGR-1016). The authors would like to acknowledge their gratitude to H. Quinteros-Lama, S. Gil-Cortizas and C. Costa-Sitjes for their assistance conducting the polar-soft SAFT modeling.

Appendix A. Supplementary data

Supplementary data to this article can be found online at https://doi.org/10.1016/j.energy.2022.124319.

References

[1] Climate & Clean Air Coalition. Our 2030 strategy - climate & clean air coalition. n.d. https://www.ccacoalition.org/en/content/our-2030-strategy. [Accessed 27 December 2021].
[2] Yang J, Sun Z, Yu B, Chen J. Modeling and optimization criteria of scroll expander integrated into organic Rankine cycle for comparison of R1233zd(E) as an alternative to R245fa. Appl Therm Eng 2018;141:386–93. https://doi.org/10.1016/J.APPLTHERMALENG.2018.06.001.
[3] Yang J, Sun Z, Yu B, Chen J. Experimental comparison and optimization guidance of R1233zd(E) as a drop-in replacement to R245fa for organic Rankine cycle application. Appl Therm Eng 2018;141:10–9. https://doi.org/10.1016/J.APPLTHERMALENG.2018.05.105.
[4] Eyerer S, Dawo F, Kaindl J, Wieland C, Spliethoff H. Experimental investigation of modern ORC working fluids R1224yd(Z) and R1233zd(E) as replacements for R245fa. Appl Energy 2019;240:946–63. https://doi.org/10.1016/J.APENERGY.2019.02.086.
[5] Yang J, Ye Z, Yu B, Ouyang H, Chen J. Simultaneous experimental comparison of low-GWP refrigerants as drop-in replacements to R245fa for Organic Rankine cycle application: R1234ze(Z), R1233zd(E), and R1336mzz(E). Energy 2019;173:721–31. https://doi.org/10.1016/J.ENERGY.2019.02.054.
[6] Petr P, Raabe G. Evaluation of R-1234ze(Z) as drop-in replacement for R-245fa in Organic Rankine Cycles – from thermophysical properties to cycle performance. Energy 2015;93:266–74. https://doi.org/10.1016/j.energy.2015.09.035.
[7] Heath EA. Amendment to the montreal Protocol on substances that deplete the ozone layer (Kigali amendment). Int Leg Mater 2017;56:193–205. https://doi.org/10.1017/ilm.2016.2.
[8] Regulation (EU. Off J Eur Union; 2014. No 517/2014 of the European Parliament and of the Council of 16 April 2014 on fluorinated greenhouse gases and repealing Regulation (EC) No 842/2006.
[9] IPCC. Climate change 2021: the physical science basis. Contribution of working group I to the sixth assessment Report of the Intergovernmental Panel on climate change. 2021.
[10] Raabe G. Molecular modeling of fluoropropene refrigerants. J Phys Chem B 2012;116:5744–51. https://doi.org/10.1021/jp300991t.
[11] Fouad WA, Vega LF. Next generation of low global warming potential refrigerants: thermodynamic properties molecular modeling. AIChE J 2018;64:250–62. https://doi.org/10.1002/aic.15859.
[12] Mota-Babiloni A, Makhnatch P, Khodabandeh R. Études récentes sur la substitution des HFC par des frigorigènes synthétiques alternatifs à faible GWP : performances énergétiques et impacts environnementaux. Int J Refrig 2017;82:288–301. https://doi.org/10.1016/j.ijrefrig.2017.06.026.
[13] Raabe G. Molecular simulation studies on refrigerants past – present – future. Fluid Phase Equil 2019;485:190–8. https://doi.org/10.1016/j.fluid.2018.12.022.
[14] Eyerer S, Wieland C, Vandersickel A, Spliethoff H. Experimental study of an ORC (Organic Rankine Cycle) and analysis of R1233zd-E as a drop-in replacement for R245fa for low temperature heat utilization. Energy 2016;103:660–71. https://doi.org/10.1016/J.ENERGY.2016.03.034.
[15] Piña-Martinez A, Lasala S, Privat R, Falk V, Jaubert J-N. Design of promising working fluids for emergent combined cooling, heating, and power (CCHP) systems. ACS Sustainable Chem Eng 2021;9:11807–24. https://doi.org/10.1021/acssuschemeng.1c03362.
[16] Husband WW, Beyene A. Low-grade heat-driven Rankine cycle, a feasibility study. Int J Energy Res 2008;32:1373–82. https://doi.org/10.1002/er.1442.
[17] Qiu G. Selection of working fluids for micro-CHP systems with ORC. Renew Energy 2012;48:565–70. https://doi.org/10.1016/J.RENENE.2012.06.006.
[18] Wang H, Li H, Wang L, Bu X. Thermodynamic analysis of organic Rankine cycle with hydrofluoroethers as working fluids. Energy Proc 2017;105:1889–94. https://doi.org/10.1016/J.EGYPRO.2017.03.554.
[19] Muñoz-Rujas N. Investigación sobre propiedades de nuevos fluidos industriales de bajo impacto ambiental como sustitutivos de gases fluorados para reducción del cambio climático. University of Burgos; 2018.
[20] Jang Y, Lee J. Optimizations of the organic Rankine cycle-based domestic CHP using biomass fuel. Energy Convers Manag 2018;160:31–47. https://doi.org/10.1016/J.ENCONMAN.2018.01.025.
[21] Vinš V, Aminian A, Celný D, Součková M, Klomfar J, Čenský M, et al. Surface tension and density of dielectric heat transfer fluids of HFE type-experimental data at 0.1 MPa and modeling with PC-SAFT equation of state and density gradient theory. Int J Refrig 2021;131:956–69. https://doi.org/10.1016/J.IJREFRIG.2021.06.029.

[22] Chapman WG, Gubbins KE, Jackson G, Radosz M. SAFT: equation-of-state solution model for associating fluids. Fluid Phase Equil 1989;52:31–8. https://doi.org/10.1016/0378-3812(89)80308-5.
[23] Blas FJ, Vega LF. Thermodynamic behaviour of homonuclear and heteronuclear Lennard-Jones chains with association sites from simulation and theory. Mol Phys 1997;92:135–50. https://doi.org/10.1080/002689797170707.
[24] Pereira LMC, Llovell F, Vega LF. Thermodynamic characterisation of aqueous alkanolamine and amine solutions for acid gas processing by transferable molecular models. Appl Energy 2018;222:687–703. https://doi.org/10.1016/J.APENERGY.2018.04.021.
[25] Pereira LMC, Vega LF. A systematic approach for the thermodynamic modelling of CO2-amine absorption process using molecular-based models. Appl Energy 2018;232:273–91. https://doi.org/10.1016/J.APENERGY.2018.09.189.
[26] Vilaseca O, Llovell F, Yustos J, Marcos RM, Vega LF. Phase equilibria, surface tensions and heat capacities of hydrofluorocarbons and their mixtures including the critical region. J Supercrit Fluids 2010;55:755–68. https://doi.org/10.1016/j.supflu.2010.10.015.
[27] Asensio-Delgado S, Jovell D, Zarca G, Urtiaga A, Llovell F. Thermodynamic and process modeling of the recovery of R410A compounds with ionic liquids. Int J Refrig 2020;118:365–75. https://doi.org/10.1016/j.ijrefrig.2020.04.013.
[28] Jovell D, Gómez S B, Zakrzewska ME, Nunes AVM, Araújo JMM, Pereiro AB, et al. Insight on the solubility of R134a in fluorinated ionic liquids and deep eutectic solvents. J Chem Eng Data 2020;65:4956–69. https://doi.org/10.1021/acs.jced.0c00588.
[29] Albà CG, Vega LF, Llovell F. A consistent thermodynamic molecular model of n-hydrofluoroolefins and blends for refrigeration applications. Int J Refrig 2020;113:145–55. https://doi.org/10.1016/J.IJREFRIG.2020.01.008.
[30] Albà C G, Alkhatib I II, Llovell F, Vega L F. Assessment of low global warming potential refrigerants for drop-in replacement by connecting their molecular features to their performance. ACS Sustainable Chem Eng 2021;9:17034–48. https://doi.org/10.1021/acssuschemeng.1c05985.
[31] Vijande J, Piñeiro MM, Bessières D, Saint-Guirons H, Legido JL. Description of PVT behaviour of hydrofluoroethers using the PC-SAFT EOS. Phys Chem Chem Phys 2004;6:766–70. https://doi.org/10.1039/B312223A.
[32] Haley JD, MCabe C. Predicting the phase behavior of fluorinated organic molecules using the GC-SAFT-VR equation of state. Fluid Phase Equil 2017;440:111–21. https://doi.org/10.1016/j.fluid.2017.01.013.
[33] Oyewunmi OA, Taleb AI, Haslam AJ, Markides CN. On the use of SAFT-VR Mie for assessing large-glide fluorocarbon working-fluid mixtures in organic Rankine cycles. Appl Energy 2016;163:263–82. https://doi.org/10.1016/J.APENERGY.2015.10.040.
[34] White MT, Oyewunmi OA, Chatzopoulou MA, Pantaleo AM, Haslam AJ, Markides CN. Computer-aided working-fluid design, thermodynamic optimisation and thermoeconomic assessment of ORC systems for waste-heat recovery. Energy 2018;161:1181–98. https://doi.org/10.1016/J.ENERGY.2018.07.098.
[35] van Kleef LMT, Oyewunmi OA, Markides CN. Multi-objective thermoeconomic optimization of organic Rankine cycle (ORC) power systems in waste-heat recovery applications using computer-aided molecular design techniques. Appl Energy 2019;251:112513. https://doi.org/10.1016/J.APENERGY.2019.01.071.
[36] Alkhatib III, Pereira LMC, Torne J, Vega LF. Polar soft-SAFT: theory and comparison with molecular simulations and experimental data of pure polar fluids. Phys Chem Chem Phys 2020;22:13171–91. https://doi.org/10.1039/D0CP00846J.
[37] Frenkel M, Chirico R, Diky V, Muzny C, Lemmon E, Yan X, et al. ThermoData engine (TDE) version 2.0 (pure compounds with EOS support); NIST standard reference database #10. 1970.
[38] Kondo S, Urano Y, Takizawa K, Takahashi A, Tokuhashi K, Sekiya A. Flammability limits of multi-fluorinated compounds. Fire Saf J 2006;41:46–56. https://doi.org/10.1016/J.FIRESAF.2005.08.002.
[39] 3M Company. Technical Data 3M Novec 7000 engineered fluid product information. n.d. https://multimedia.3m.com/mws/media/121372O/3m-novec-7000-engineered-fluid-tds.pdf&fn=3M Novec 7000 Engineered Fluid TDS Heat Transfer_FINAL_R3.pdf. [Accessed 12 November 2021].
[40] 3M Company. Technical Data 3M Novec 7100 engineered fluid product information. n.d. https://multimedia.3m.com/mws/media/199818O/3m-novec-7100-engineered-fluid.pdf&fn=prodinfo_nvc7100.pdf. [Accessed 12 November 2021].
[41] 3M Company. Technical Data 3M Novec 7200 engineered fluid product information. n.d. https://multimedia.3m.com/mws/media/199819O/3m-novec-7200-engineered-fluid-en.pdf&fn=prodinfo_nvc7200.pdf. [Accessed 12 November 2021].
[42] Company 3M.. Technical Data 3M Novec 7300 engineered fluid product information. n.d. https://multimedia.3m.com/mws/media/338713O/3m-novec-7300-engineered-fluid.pdf. [Accessed 12 November 2021].
[43] 3M Company. Technical Data 3M Novec 7500 engineered fluid product information. n.d. https://multimedia.3m.com/mws/media/65496O/3m-novec-7500-engineered-fluid.pdf&fn=prodinfo_nvc7500.pdf. [Accessed 12 November 2021].
[44] Demuth OJ. Preliminary assessment of condensation behavior for hydrocarbon-vapor expansions which cross the saturation line near the critical point. Idaho Falls (USA): EG and G Idaho, Inc.; 1983.
[45] Hung TC. Waste heat recovery of organic Rankine cycle using dry fluids. Energy Convers Manag 2001;42:539–53. https://doi.org/10.1016/S0196-8904(00)00081-9.
[46] Chen H, Goswami DY, Stefanakos EK. A review of thermodynamic cycles and working fluids for the conversion of low-grade heat. Renew Sustain Energy Rev 2010;14:3059–67. https://doi.org/10.1016/J.RSER.2010.07.006.
[47] Wang Q, Wu W, He Z. Thermodynamic analysis and optimization of a novel organic Rankine cycle-based micro-scale cogeneration system using biomass fuel. Energy Convers Manag 2019;198:111803. https://doi.org/10.1016/J.ENCONMAN.2019.111803.
[48] Chapman WG, Gubbins KE, Jackson G, Radosz M. New reference equation of state for associating liquids. Ind Eng Chem Res 1990;29:1709–21. https://doi.org/10.1021/ie00104a021.
[49] Gubbins KE, Twu CH. Thermodynamics of polyatomic fluid mixtures—I theory. Chem Eng Sci 1978;33:863–78. https://doi.org/10.1016/0009-2509(78)85176-8.
[50] Twu CH, Gubbins KE. Thermodynamics of polyatomic fluid mixtures—II: polar, quadrupolar and octopolar molecules. Chem Eng Sci 1978;33:879–87. https://doi.org/10.1016/0009-2509(78)85177-X.
[51] Jog PK, Chapman WG. Application of Wertheim's thermodynamic perturbation theory to dipolar hard sphere chains. Mol Phys 1999;97:307–19. https://doi.org/10.1080/00268979909482832.
[52] Stell G, Rasaiah JC, Narang H. Thermodynamic perturbation theory for simple polar fluids, I. Mol Phys 1972;23:393–406. https://doi.org/10.1080/00268977200100381.
[53] Luckas M, Lucas K, Deiters U, Gubbins KE. Integrals over pair- and triplet-correlation functions for the Lennard-Jones (12–6)-fluid. Mol Phys 1986;57:241–53. https://doi.org/10.1080/00268978600100191.
[54] Balasubramani SG, Chen GP, Coriani S, Diedenhofen M, Frank MS, Franzke YJ, et al. TURBOMOLE: modular program suite for ab initio quantum-chemical and condensed-matter simulations. J Chem Phys 2020;152:184107. https://doi.org/10.1063/5.0004635.
[55] Dassault Systèmes. BIOVIA COSMOtherm. n.d. http://www.3ds.com. [Accessed 8 November 2021].
[56] Hait D, Head-Gordon M. How accurate is density functional theory at predicting dipole moments? An assessment using a new database of 200 benchmark values. J Chem Theor Comput 2018;14:1969–81. https://doi.org/10.1021/acs.jctc.7b01252.
[57] Cahn JW, Hilliard JE. Free energy of a nonuniform system. I. Interfacial free energy. J Chem Phys 1958;28:258–67. https://doi.org/10.1063/1.1744102.
[58] Waals JD van der. Thermodynamische Theorie der Kapillarität unter Voraussetzung stetiger Dichteänderung. Zeitschrift Für Phys Chemie 1894;13U:657–725. https://doi.org/doi:10.1515/zpch-1894-1338.
[59] Mejía A, Segura H. Interfacial behavior in type IV systems. Int J Thermophys 2004;25:1395–414. https://doi.org/10.1007/s10765-004-5746-9.
[60] Vilaseca O, Vega LF. Direct calculation of interfacial properties of fluids close to the critical region by a molecular-based equation of state. Fluid Phase Equil 2011;306:4–14. https://doi.org/10.1016/j.fluid.2010.09.018.
[61] Pàmies JC. Bulk and interfacial properties of chain fluids a molecular modelling approach : tesis doctoral. Universitat Rovira i Virgili; 2003.
[62] Murata J, Yamashita S, Akiyama M, Katayama S, Hiaki T, Sekiya A. Vapor pressures of hydrofluoroethers. J Chem Eng Data 2002;47:911–5. https://doi.org/10.1021/je010322y.
[63] Rausch MH, Kretschmer L, Will S, Leipertz A, Fröba AP. Density, surface tension, and kinematic viscosity of hydrofluoroethers HFE-7000, HFE-7100, HFE-7200, HFE-7300, and HFE-7500. J Chem Eng Data 2015;60:3759–65. https://doi.org/10.1021/acs.jced.5b00691.
[64] Lemmon EW, Bell IH, Huber ML, McLinden MO. NIST standard reference database 23: reference fluid thermodynamic and Transport properties-REFPROP, version 10.0. National Institute of Standards and Technology; 2018.
[65] Yasumoto M, Yamada Y, Murata J, Urata S, Otake K. Critical parameters and vapor pressure measurements of hydrofluoroethers at high temperatures. J Chem Eng Data 2003;48:1368–79. https://doi.org/10.1021/je0201976.
[66] Goodwin A RH, Defibaugh D R, Weber L A, Goodwin ARH, Defibaugh DR, Weber LA. Vapor pressure of 2-(Difluoromethoxy)-1,1,1-trifluoroethane CHF2−O−CH2CF3 (HFE-245). J Chem Eng Data 1998;43:846–8. https://doi.org/10.1021/je980056x.
[67] Kayukawa Y, Hasumoto M, Hondo T, Kano Y, Watanabe K. Thermodynamic property measurements for trifluoromethyl methyl ether and pentafluoroethyl methyl ether. J Chem Eng Data 2003;48:1141–51. https://doi.org/10.1021/je025657+.
[68] Chen Q, Du L, Guan X, Guo Z, Gao R, Li W, et al. Measurement of saturated vapor pressure and compressed liquid density for 1,1,1,3,3,3-hexafluoroisopropylmethyl ether. J Chem Eng Data 2020;65:4790–7. https://doi.org/10.1021/acs.jced.0c00232.
[69] Ohta H, Morimoto Y, Widiatmo JV, Watanabe K. Liquid-phase thermodynamic properties of new refrigerants: pentafluoroethyl methyl ether and heptafluoropropyl methyl ether. J Chem Eng Data 2001;46:1020–4. https://doi.org/10.1021/je0002538.
[70] Ripple D, Matar O. Viscosity of the saturated liquid phase of six halogenated compounds and three mixtures. J Chem Eng Data 1993;38:560–4. https://doi.org/10.1021/je00012a021.
[71] Pàmies J C, Vega L F. Vapor−Liquid equilibria and critical behavior of heavy n-alkanes using transferable parameters from the soft-SAFT equation of state. Ind Eng Chem Res 2001;40:2532–43. https://doi.org/10.1021/ie000944x.
[72] Quoilin S, Broek M Van Den, Declaye S, Dewallef P, Lemort V. Techno-

economic survey of organic rankine cycle (ORC) systems. Renew Sustain Energy Rev 2013;22:168–86. https://doi.org/10.1016/J.RSER.2013.01.028.
[73] Sekiya A, Misaki S. The potential of hydrofluoroethers to replace CFCs, HCFCs and PFCs. J Fluor Chem 2000;101:215–21. https://doi.org/10.1016/S0022-1139(99)00162-1.
[74] Muñoz-Rujas N, Aguilar F, García-Alonso JM, Montero EA. High pressure density and speed of sound of hydrofluoroether fluid 1,1,1,2,2,3,4,5,5,5-decafluoro-3-methoxy-4-(trifluoromethyl)-pentane (HFE-7300). J Chem Thermodyn 2018;121:1–7. https://doi.org/10.1016/J.JCT.2018.02.003.
[75] Alkhatib III, Vega LF. Quantifying the effect of polarity on the behavior of mixtures of n-alkanes with dipolar solvents using polar soft-statistical associating fluid theory (Polar soft-SAFT). AIChE J 2021;67:e16649. https://doi.org/10.1002/aic.16649.
[76] Hiaki T, Kawai A. Vapor–liquid equilibria determination for a hydrofluoroether with several alcohols. Fluid Phase Equil 1999;158–160:979–89. https://doi.org/10.1016/S0378-3812(99)00064-3.
[77] Tochigi K, Satou T, Kurihara K, Ochi K, Yamamoto H, Mochizuki Y, et al. Vapor–Liquid equilibrium data for the four binary systems containing fluorocarbon, hydrofluorocarbon, and fluorinated ethers at 101.3 kPa. J Chem Eng Data 2001;46:913–7. https://doi.org/10.1021/je000192d.
[78] Řehák K, Klajmon M, Strejc M, Morávek P. Isothermal vapor–liquid equilibria for binary mixtures of methyl nonafluorobutyl ether + acetone, cyclopentyl methyl ether, ethyl acetate, n-heptane, methanol, and toluene. J Chem Eng Data 2017;62:3878–88. https://doi.org/10.1021/acs.jced.7b00599.
[79] Tchanche BF, Lambrinos G, Frangoudakis A, Papadakis G. Low-grade heat conversion into power using organic Rankine cycles – a review of various applications. Renew Sustain Energy Rev 2011;15:3963–79. https://doi.org/10.1016/J.RSER.2011.07.024.
[80] Albornoz J, Mejía A, Quinteros-Lama H, Garrido JM. A rigorous and accurate approach for predicting the wet-to-dry transition for working mixtures in organic Rankine cycles. Energy 2018;156:509–19. https://doi.org/10.1016/J.ENERGY.2018.05.074.
[81] Garrido JM, Quinteros-Lama H, Mejía A, Wisniak J, Segura H. A rigorous approach for predicting the slope and curvature of the temperature–entropy saturation boundary of pure fluids. Energy 2012;45:888–99. https://doi.org/10.1016/J.ENERGY.2012.06.073.